J. Cent. South Univ. (2021) 28: 2485−2498
DOI: https://doi.org/10.1007/s11771-021-4781-z

Springer

Influence of infilling stiffness on mechanical and fracturing responses of hollow cylindrical sandstone under uniaxial compression tests

WU Qiu-hong(吴秋红)[1], WENG Lei(翁磊)[2, 3], ZHAO Yan-lin(赵延林)[1], FENG Fan(冯帆)[3]

1. Work Safety Key Lab on Prevention and Control of Gas and Roof Disasters for Southern Coal Mines, Hunan Provincial Key Laboratory of Safe Mining Techniques of Coal Mines, Hunan University of Science and Technology, Xiangtan 411201, China;
2. School of Civil Engineering, Wuhan University, Wuhan 430072, China;
3. Key Laboratory of Mining Disaster Prevention and Control, Shandong University of Science and Technology, Qingdao 266590, China

Abstract: Hollow cylindrical sandstone specimens filled with Al, Pb and polymethyl methacrylate (PMMA), as well as hollow and solid specimens were tested under monotonic unconfined compression. The discrepancies in the elastic modulus, unconfined compressive strength and failure pattern of the specimens were studied and then illustrated. The interaction stress threshold and localized failure stress threshold were identified by the strain gauges on the rock and filling rod. The results indicated that unobvious changes in the strength and elastic modulus were found between the solid and hollow specimens, while for the hollow specimens with infillings, the strength decreases with increasing the stiffness of the infilling material. The filling material with a higher stiffness leads to a high hoop stress, and hence a stronger interfacial force. The specimens coupled with filling rod are mainly fractured with tensile cracks, while the solid and hollow specimens are typically split into blocky fragments with dominated shear fractures. Finally, the equivalent inner pressure in the opening was theoretically derived. The findings suggested in the experiments can be well explained using the theoretical thick-walled cylinder model.

Key words: mechanical properties; hollow cylinder; infilling; hoop stress; uniaxial compression

Cite this article as: WU Qiu-hong, WENG Lei, ZHAO Yan-lin, FENG Fan. Influence of infilling stiffness on mechanical and fracturing responses of hollow cylindrical sandstone under uniaxial compression tests [J]. Journal of Central South University, 2021, 28(8): 2485−2498. DOI: https://doi.org/10.1007/s11771-021-4781-z.

1 Introduction

Conventional axisymmetric tests, such as the uniaxial and triaxial compression tests, on standard cylindrical specimens are one of the simplest and the most widely used methods to investigate the mechanical behaviors and properties of rock [1−5]. By conducting the conventional compression tests, one can obtain the mechanical parameters of rock [6−9], for instance, the compressive strength, elastic modulus and Poisson ratio. These parameters can be easily derived from the readings of the loading cell and strain gauges [10−12]. The test schemes, however, is somewhat inadequate to mimic the stress conditions encountered in situ, particularly in the rock surroundings in which excavated openings are existed [13, 14]. For example, the geo-stresses

Foundation item: Projects(51904101, 51774131, 52004143) supported by the National Natural Science Foundation of China; Project(MDPC201916) supported by the Key Laboratory of Mining Disaster Prevention and Control, China
Received date: 2020-07-22; **Accepted date:** 2021-01-17
Corresponding author: WENG Lei, PhD; Tel: +86-17671467186; E-mail: leiweng@whu.edu.cn; ORCID: https://orcid.org/0000-0002-2981-5110; FENG Fan, PhD; Tel: +86-15610569187; E-mail: fengfan0213@sdust.edu.cn; ORCID: https://orcid.org/0000-0002-8239-1484

around the opening are in fact distributed in a non-uniform manner, making the deformation and failure of the surrounding rock extremely complicated [15−19]. Therefore, investigations on the mechanical behaviors of rock under non-uniform stresses are of great importance to underground engineering [20, 21].

In this regard, the form of hollow cylinder was used to reproduce complicated stress conditions in laboratory with an attempt to simulate the stress state in field [22−27]. Pioneering works have been initiated using the hollow cylinder specimens to study the deformation and fracture characteristics of underground openings since 1912 [28, 29]. With different combinations of the axial load, confining pressure and inner pressure, a wide variety of stress paths can be achieved, for example the true three-dimensional stresses [13] and true triaxial stresses with torsion force [30]. Testing on hollow cylinders has two prominent merits. One is that tests using hollow cylinders can better mimic the geo-stress conditions around deep well bores or openings in engineering practice [31, 32]. The other advantage is that tests using hollow cylinders can evaluate the mechanical behaviors of rock specimens, and perform physical simulation analysis at reduced scale for many rock engineering applications [13, 24, 25]. In this regard, extensive works were performed on hollow cylindrical specimens in the aim of understanding the mechanical behaviors and failure characteristics of rock. For instance, GAY [33] carried out a series of experiments using homogenous sandstone and anisotropic clay quartzite with pre-cut circular, elliptic and square holes. ALSAYED [13] performed various tests on samples of spring well sandstone subjected to various stress paths. YOU et al [34] investigated the effect of the hole size on the strength and failure modes of hollow cylinders. ZHANG et al [35] performed loading and unloading tests to study the mechanism of ring-like failure using relative larger hollow cylinders. LABIOUSE et al [36] investigated the effect of excavation on nuclear waste disposal using hollow cylinderical clay specimens. LI et al [37] developed hollow cylinder apparatuses to study the mechanical properties of rock under comprehensive stress paths. Additionally, YANG [24] investigated the effect of the hole diameter on the deformation, strength and cracking behaviors of the hollow sandstone specimens under different confining pressures. WU et al [25] studied the failure behaviors of hollow cylinder specimens under complex stress conditions, and examined the different failure mechanisms in detail. WANG et al [26] investigated the influence of the radial stress gradient, external confining stress and specimen length-to-diameter ratio on the triaxial compressive strength. The abovementioned previous works have greatly promoted the understanding of the relations of the stress paths with the mechanical properties and failure patterns of rock [38−40]. However, few focused on the relationship between the deformation and strength characteristics of the surrounding rock and the filling material.

Tests on hollow cylinder specimens with fillings can conveniently obtain different internal pressures on the opening wall, but also are beneficial for studying the interaction of the rock with filling material because the deformation of the filling is compiled with that of the rock structure [41]. This paper aims to investigate the mechanical properties and failure behaviours of hollow cylindrical sandstones with different filling materials. The filling materials were made of aluminium (Al), lead (Pb) and polymethyl methacrylate (PMMA), respectively, which had different stiffnesses and strengths. The fillings-rock coupled specimens were loaded monotonically till failure. The derivations of the elastic modulus, unconfined compressive strength and failure mode have been analyzed. The hoop stress at the interface between the rock and the filling material was derived using strain gauge measurement. Finally, a theoretical model was established to illustrate experimental phenomena.

2 Materials and methods

2.1 Rock specimen collection

The sandstone specimens for experimentation were sourced from a sandstone quarry in Changlong, Sichuan province of China. The rock blocks were extracted from the host rock by a machine cutting technique, so that the minimum artificial damage was induced to both the remaining rock mass and block, which was beneficial for experimental investigation. A visual inspection showed that the sandstone is consisted mainly of quartz and albite with no obvious “defects”, and the average grain size is approximately 1.0 mm.

The sandstone cylinders with 74 mm in

diameter and 148 mm in height were first cored from the rock block. Then the solid cylinders were further processed into hollow cylinders having an inner diameter of 20 mm. Finally, a round rod with a diameter of 19 mm and height of 144 mm was filled into the hole, and was glued with the wall surface using an universal adhesive. Three kinds of rod materials having different stiffnesses, for example the aluminium, lead and PMMA were taken into account in this study. The rod was positioned at the centre of the inner hole so that both ends of the rod were approximately 2.0 mm shorter than the specimen end (Figure 1). Such a configuration ensures the filling rod did not directly contact with the loading platen. Therefore, the filling rod was exempt from the direct force by the platen, which is beneficial for investigating the interaction of the filling rod with the rock structure. It should be noted that the diameter of the sandstone cylinder is 74 mm, which is larger than that as recommended by the International Society for Rock Mechanics (ISRM) testing suggested method (i.e., 50 mm). Since the specimen tested in study is hollowed out and then will be infilled with other material so as to investigate the filling effect. A larger size of the specimen is beneficial to improve the support capacity of the filling material and to achieve favorable experimental results. Although the diameter of the specimen is larger than 50 mm, the height-to-diameter ratio is 2.0, which conforms to the ISRM testing suggested method.

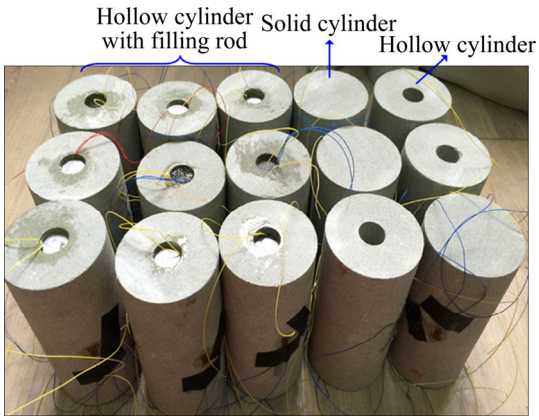

Figure 1 Test specimen with different filling materials

The specimens were grouped into five sets according to their geometric configurations and the filling materials, i.e. solid cylinder (SC), hollow cylinder (HC), hollow cylinder filled with aluminium (HC-Al), hollow cylinder filled with lead (HC-Pb) and hollow cylinder filled with PMMA (HC-PMMA). The density of sandstone ranges from 2268.7 to 2383.1 kg/m^3 with a variation coefficient of 1.3%, and the P-wave velocity ranges from 2300.7 to 2650.7 m/s having a variation coefficient of 3.9%. Both the variation coefficients are small and limited, indicating that the test specimens are relative homogeneous. The uniaxial compressive strength (UCS) of the sandstone is 71.0 MPa averaged from three solid specimens under uniaxial compression tests. The tensile strength of the sandstone is obtained to be 2.3 MPa based on the Brazilian disc test.

The physical properties of the filling materials are listed in Table 1. It is observed that the aluminium rod has the highest elastic modulus (i.e. stiffness), followed by the lead rod and then PMMA. The yield strength, however, is much different among the three filling materials. Specifically, the yield strength for PMMA reaches as high as 98 MPa, which is approximately 3 times of the aluminium and 40 times of the lead. These different infilling materials with distinguishing mechanical parameters will exhibit various interactions with the rock, which is the aim of this study.

Table 1 Basic physical and mechanical properties of rock and filling materials

Material	Density/ (kg·m^{-3})	P-wave velocity/ (m·s^{-1})	Elastic modulus/ GPa	Poisson ratio	Yield strength/ MPa
Sandstone	2354	2360	12.3	0.28	—
Aluminium	2700	6300	70	0.3	30
Lead	11343	2200	17	0.42	2.5
PMMA	1190	1700	3	0.37	98

2.2 Test methods

Monotonic unconfined compression tests were conducted with the help of a servo-controlled RMT150-C system. The value of axial stress was obtained by the reading of loading cell, and the axial strain was the overall strain of the sample measured by a linear variable differential transformer (LVDT), which recorded the movement of the loading piston. Model DH3820 strain gauge system was used to record the local strains of the specimen and filling rod. Three strain gauges were stuck on the specimen: two (SG-1and SG-3, model BX120-3AA) were placed on the outer surface of the specimen to trace the axial and lateral strains, while the other one

(SG-2, model BX120-1AA) was positioned on the face of the filling rod to trace the lateral strain. A displacement control module was used to loading the specimen at a loading speed of 0.3 mm/min till failure. Figure 2 presents the configuration of the loading cell.

3 Experimental results

3.1 Stress−strain relations

Figure 3 shows the stress−strain curves of the five groups of specimens having different infillings and geometric configurations. For each case, the specimen typically experiences four deformation

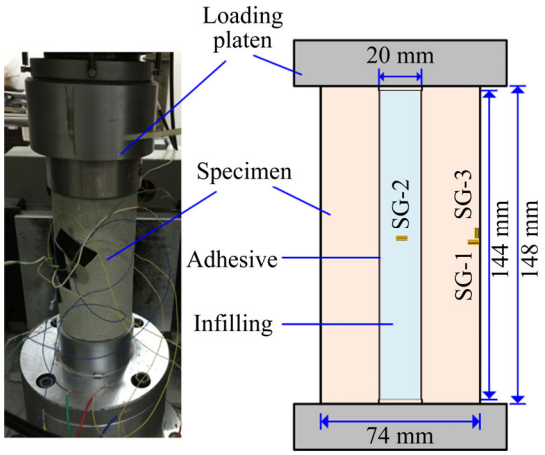

Figure 2 Configuration of loading cell and specimen

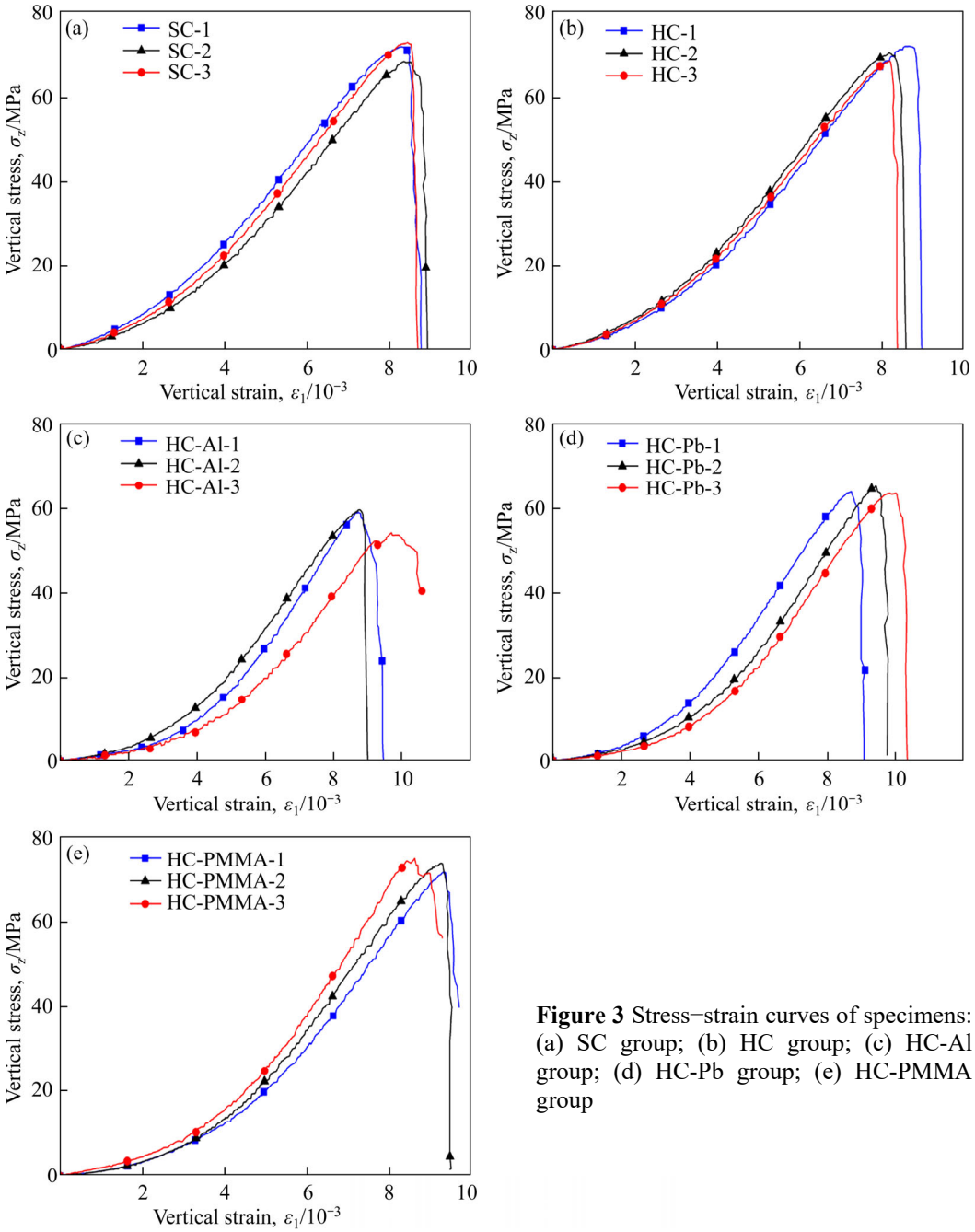

Figure 3 Stress−strain curves of specimens: (a) SC group; (b) HC group; (c) HC-Al group; (d) HC-Pb group; (e) HC-PMMA group

stages, i.e. the compaction, elastic deformation, yielding and post peak stages in the process of uniaxial compression till failure. The maximum principal stress drops immediately at the onset of the specimen failure, indicating that the specimen exhibit obvious brittle manners, irrespective of the infillings. Alternatively, the overall deformation behaviors were not affected by the inner filling rods probably because the filling rod was not directly contacted with the loading platen, as abovementioned in Section 2.1. In this regard, the stresses applied on the filling rod were mainly induced by the interfacial friction and the radial expansion of the rock, which were much smaller than the loading stress. Therefore, the interaction between the filling rod and the rock is less pronounced than the mechanical behaviors of rock under compression.

Figure 4 presents the changes in unconfined compressive strength (UCS) for the five groups of specimens. It can be observed that the UCS of the solid specimen is approximately equal to that of the hollow specimen. This phenomenon is in agreement with the result in Ref. [42]. However, the strength of the specimens with infillings significantly varies with one another, depending on the stiffness of the filling rods. For instance, as for the hollow specimen filled with aluminium, the average UCS reduces to 57.5 MPa, which is 17.9% lower than of the hollow specimen without infilling. Similarly, the average UCS of the Pb-filled specimen is 8.9% lower than that of the hollow specimen. Nevertheless, the average UCS of the PMMA-filled specimen is 73.1 MPa, which is 4.4% higher than the UCS of hollow specimen. This phenomenon indicates that the strength of the filled cylinder decreases with the increase in the stiffness of the filling material.

Figure 5 presents the changes in elastic modulus

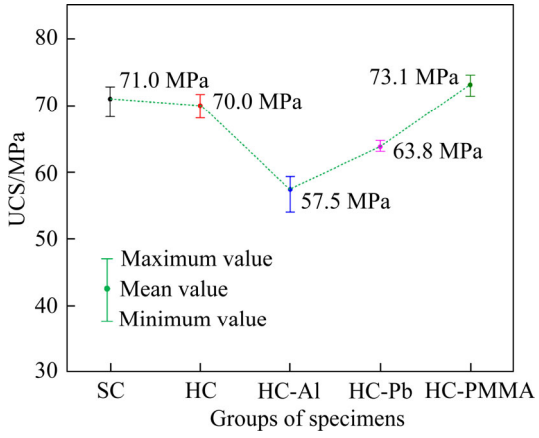

Figure 4 Changes in UCS for specimens

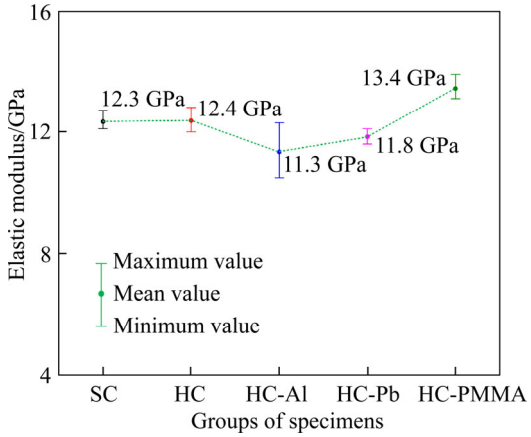

Figure 5 Changes in elastic modulus for specimens

for the five groups of specimens with different infillings. It can be observed that the HC-PMMA specimen has the highest elastic modulus, whereas the HC-Al specimen has the lowest elastic modulus. The elastic modulus of the SC specimen is nearly the same as the elastic modulus of the HC specimen, indicating that the empty hole does not significantly influence the deformation of the hollowed sandstone. However, with filled materials, the hollowed specimens exhibit obvious distinct elastic modulus depending on the stiffness and strength of the infillings. The HC specimen with filling material having a higher stiffness exhibits a lower elastic modulus. Such a phenomenon occurs because of the interaction of the sandstone and the infilling material.

The elastic modulus variation trend shown in Figure 5 is similar to the changes in the strength as observed in Figure 4. However, the differences in elastic modulus among the five groups of specimens are minor. For instance, the gap between the highest and the lowest elastic modulus is only 2.1 GPa, indicating that the elastic modulus of the hollow specimen with infillings is affected by the filling stiffness similar to the strength but to a less extent.

3.2 Deformation behaviors

To illustrate the deformation behaviors of the rock and filling rod and their interactions, Figure 6 presents the curves of axial stress and SG readings against loading time for the specimen HC-Al-2 (Figure 6(a)), HC-Pb-3 (Figure 6(b)) and HC-PMMA-3 (Figure 6(c)). The reading of SG-1 denotes the lateral strain on the outer surface of the specimen, and the reading of SG-2 represents the lateral strain on the filling rod. Figure 7 shows the

curves of SG-1 reading versus loading time of the specimens. Since the SG-2 was sandwiched between the surfaces of the filling rod and inner wall of rock, the evolution of SG-2 clearly reflected the interaction of the filling rod with the rock structure. As shown in Figure 6, the typical curves exhibit similar trend in demonstrating the deformation behaviors of the rock and filling rod. The values on the green arrow line denote the strain reading of SG-2 at the selected moments. For instances, the lateral strain reading recorded by SG-1 increases slowly at the primary loading stage, and then speeds

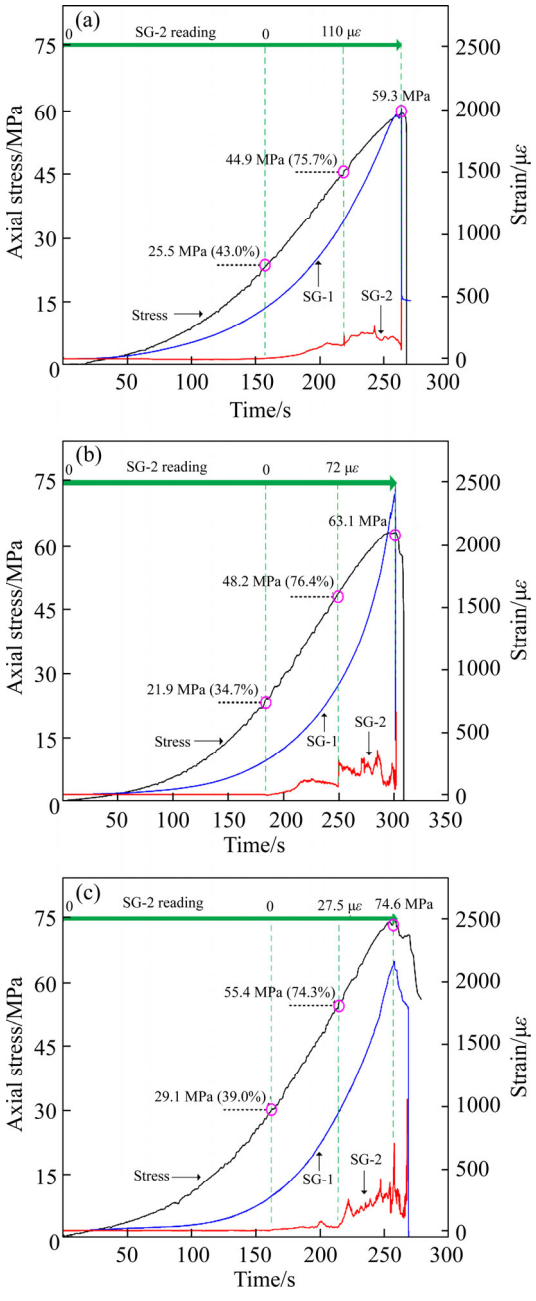

Figure 6 Typical curves of axial stress and SG readings against time for specimens HC-Al-2 (a), HC-Pb-3 (b) and HC-PMMA-3(c)

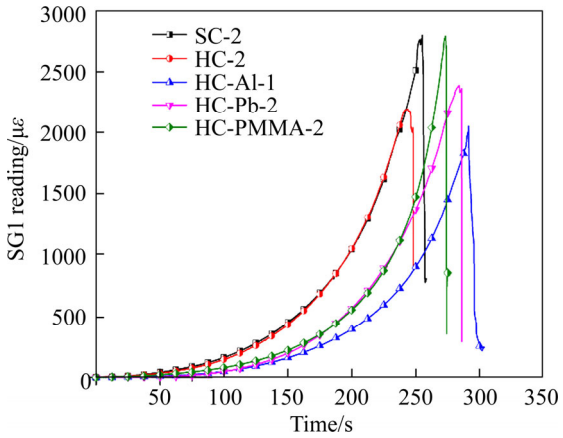

Figure 7 Typical curves of SG-1 reading for specimens

up in a non-linear manner till failure (also see Figure 7), which is in good accordance to the overall deformation process of the rock. The peak strain on the SG-1 reading curve shows a coherent variation trend with those indicated in Figures 4 and 5. Particularly, a reduction of the lateral peak strain with increasing the stiffness of the filling rod can be observed.

On the other hand, it can be observed that the SG-2 reading remains zero during the early loading stage, indicating that the filling rod has not yet interacted with the rock structure at such a stress level. When the axial stress reaches to a certain level, for example 43% UCS of the specimen HC-Al-2, 34.7% UCS of the specimen HC-Pb-3 and 39% UCS of the specimen HC-PMMA-3 (see Figures 6(a)−(c)), the SG-2 reading starts to increase rapidly. At this stress level, the filling rod begins to interact with the rock structure, and exerts influence on the mechanical behaviors of the rock. This stress threshold is identified to be the stress-to-interact (σ_{ite}). With further increasing the loading stress, the SG-2 reading shows a dramatic increase at 75.7 % of the peak stress for specimen HC-Al-2, 76.4% of the peak stress for specimen HC-Pb-3 and 74.3% of the peak stress for specimen HC-PMMA-3, respectively. The significant change in SG-2 reading indicates that a localized failure has been induced at the infilling-rock interface. It is seen that such a stress level is close to the yielding stress threshold, and therefore it is denoted as the localized failure stress σ_{loc}. At the yielding stage, the change tendency of the SG-2 reading goes up and down several times prior to the overall failure of the specimen.

To further illustrate the interaction of the filling rod and rock, Table 2 summarizes the interaction

Table 2 Thresholds of interaction stress and localized failure stress

Specimen	σ_{peak}/MPa	σ_{ite}/MPa	($\sigma_{ite}/\sigma_{peak}$)/%	σ_{loc}/MPa	($\sigma_{loc}/\sigma_{peak}$)/%	SG-2 reading at σ_{loc}/με
HC-Al-1	58.9	18.8	31.9	41.2	69.9	127
HC-Al-2	59.3	25.5	43.0	44.9	75.7	110
HC-Al-3	54.1	20.9	38.6	42.4	78.3	150
HC-Pb-1	63.5	25.6	40.3	49.1	77.3	87
HC-Pb-2	64.7	23.1	35.7	40.9	67.9	99
HC-Pb-3	63.1	21.9	34.7	48.2	76.4	72
HC-PMMA-1	71.4	19.4	30.0	45.5	69.3	35
HC-PMMA-2	73.4	26.6	36.2	58.8	78.7	17
HC-PMMA-3	74.6	29.1	39.0	55.4	74.3	27.5

Note: σ_{ite} denotes the stress-to-interact; σ_{loc} denotes localized failure stress; σ_{peak} denotes the peak stress.

stress threshold σ_{ite} and the localized failure stress threshold σ_{loc}, and their proportions to the peak stress for all the hollow specimens with infillings. The value of the SG-2 reading at the onset of the yielding is also included in Table 2. We can observe that the interaction stress threshold (i.e., σ_{ite}) ranges approximately between 30.0% and 43.0% of the peak stress, and the localized failure stress threshold (σ_{loc}) is generally in the range 67.9% to 78.3% of the peak stress. The interaction of the filling rod with the rock structure initiated at an early stage of elastic deformation (i.e., 0.3 times the UCS according to Ref. [43] and the localized failure occurred at the end of the elastic deformation (0.7 times the UCS). This can be illustrated in Figure 4 that the curve of SG-2 reading changes smoothly prior to the localized failure stress threshold, while it fluctuates fiercely at the yielding stage.

Table 2 also shows that the SG-2 reading of PMMA infilling is much lower than those of lead and aluminium infillings, which indicates that the deformation of PMMA is comparatively smaller from the onset of the filling-rock interaction to the yielding point. In contrast, the aluminium filling rod experienced the largest deformation, indicating that larger stress was probably induced between the infilling-rock interface. To verify this phenomenon, the hoop stress of the filling rod was obtained via multiplying SG-2 value by elastic modulus of the filling material. The approach to calculate the hoop stress can be justified owing to the fact that the filling material is homogeneous and has the same elastic modulus in all directions. Figure 8 shows the curves of hoop stress against loading time for the specimens HC-Al-2, HC-Pb-3 and HC-PMMA-3. We can observe that the hoop stress of the aluminium rod

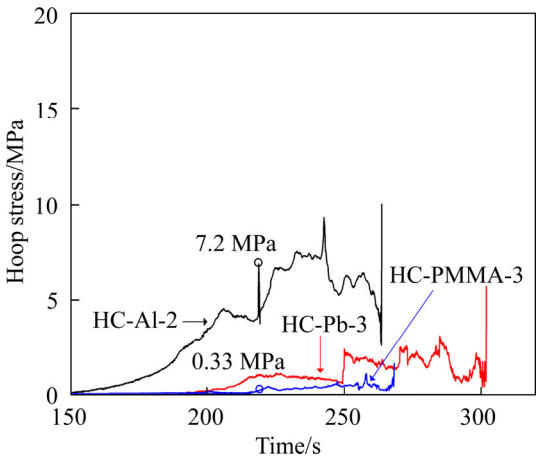

Figure 8 Typical curves of hoop stress against time

reaches 8.2 MPa prior to the onset of localized failure, whereas the hoop stress of the PMMA rod is merely 0.33 MPa. It is indicated that much higher hoop stress could be induced in the filling material with higher elastic modulus, and hence leads to a stronger interfacial stress. Under this case, the specimen is prone to be damaged due to the excess inner stress. This finding explains the phenomenon that a higher stiffness of the infilling leads to lower UCS and elastic modulus of the filled hollow specimen, as shown in Figures 4 and 5.

3.3 Failure modes

Figure 9 presents typical failure modes of the specimens under uniaxial compression. The solid and hollow specimens were fractured into small blocks with mixed fracture-tensile planes. Meanwhile, shear fracture mainly dominates the failure pattern and minor local tensile failures can be also observed on the specimen. However, the failure modes between the solid and hollow specimens show unclear discrepancies, which is probably due to the

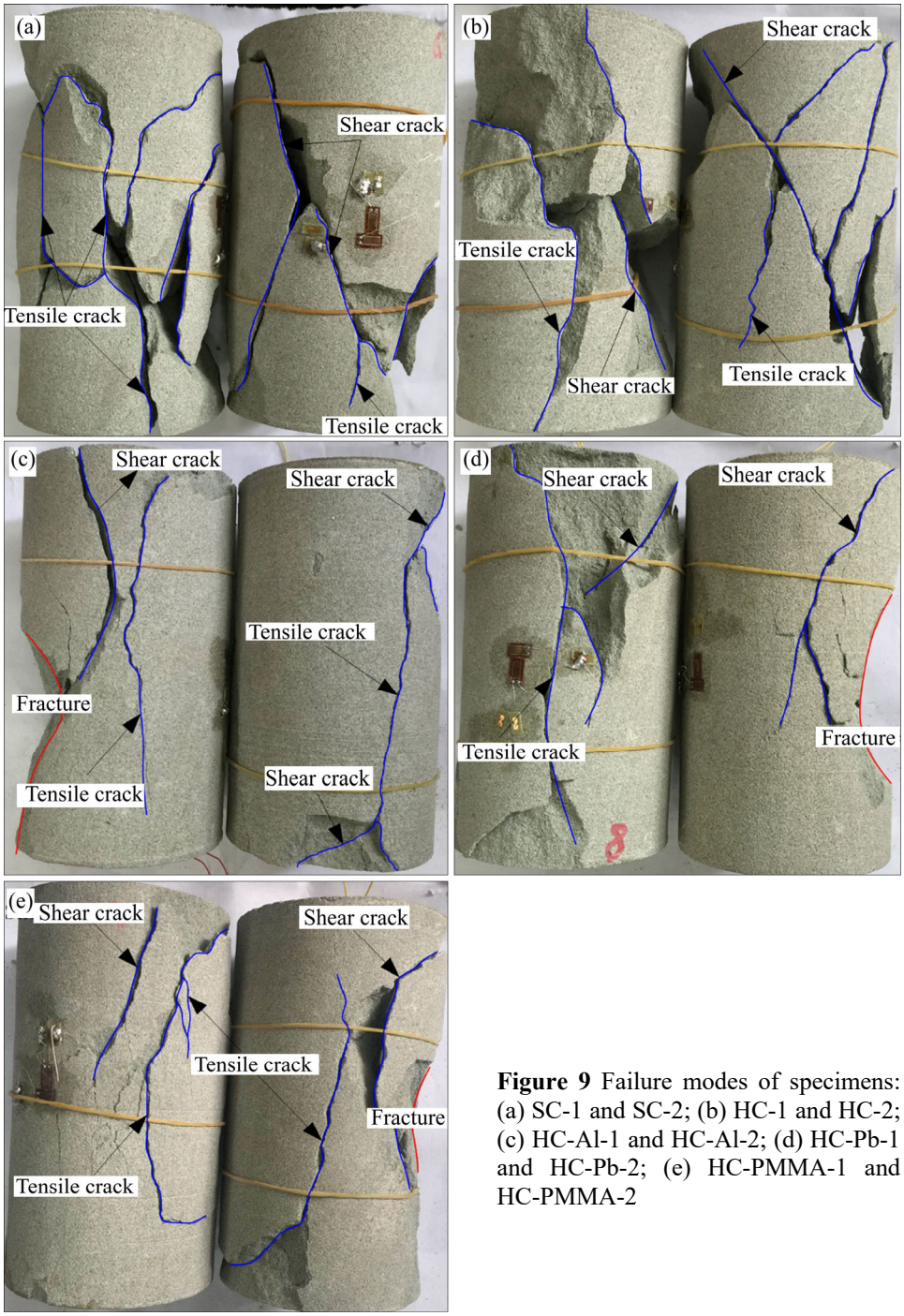

Figure 9 Failure modes of specimens: (a) SC-1 and SC-2; (b) HC-1 and HC-2; (c) HC-Al-1 and HC-Al-2; (d) HC-Pb-1 and HC-Pb-2; (e) HC-PMMA-1 and HC-PMMA-2

small inner diameter. As indicated by YOU et al [34] and GOU et al [42], a small ratio of the inner diameter to outer diameter for hollow specimen resulted in a tiny effect on the mechanical behavior. In terms of the hollow specimens with different infillings, the failure patterns exhibit clear derivations. For instance, the specimen coupled with a filling rod is typically fractured with tensile cracks as can be observed on the surface, and few shear cracks can be also inspected. Furthermore, the specimens were not split into blocky fragments compared with the solid and hollow specimens. The reason for such a phenomenon may be attributed to the function of the filling rod. The carrying-capacity of the specimen was reinforced by the filling rod which provided not only a radial constraint but also an axial friction force to the rock structure.

4 Theoretical analyses and discussion

In this paper, to understand how the filling material influences the mechanical and failure

behaviors of hollow specimen, we conducted monotonic unconfined compression tests on hollow cylinder specimens with varying infillings. The results indicated that the filling material has little effect on the elastic modulus of the specimen, while it plays a significant role in changing the strength of the specimen. With the increase in the stiffness of the filling rod, the unconfined compressive strength clearly decreases. The results in Figure 8 also indicate that the filling rod with a higher stiffness induces a higher hoop stress between the interface of the rock and infilling. Therefore, the mechanical behaviors of hollow specimen with infillings are much related to the interaction of the rock structure with the filling materials, as also illustrated by WU et al [44].

The interaction initiated at the axial stress level of approximately 30% to 43% UCS, and was disturbed by localized failure at the inner wall at the stress level of 67.9% to 78.3% UCS. This phenomenon generally occurred at the elastic deformation stage of the specimen, in which the interfacial stresses were generated during the deformation of the rock and filling rod. To illustrate this problem, a thick-walled cylinder model was established as presented in Figure 10. The force generated at the interface between the rock and filling rod could be divided into two parts, i.e., a friction force (f) along the axial direction and an inner pressure vertically oriented to the wall. Because the filling rod was not directly subjected to the axial stress by loading platen, the friction force was small and could be ignored in this case. This simplification could be also justified due to the fact that the relative movement of the rock and filling rod was extremely small prior to the rock failure, which contributes to a very small friction force between their interfaces. Therefore, according to the theory of elastic mechanics, the stresses in the hollow cylinder could be expressed as follows [45]:

$$\sigma_\theta = -\frac{r_1^2 r_2^2 P_i}{r_2^2 - r_1^2}\frac{1}{r^2} - \frac{r_1^2 P_i}{r_2^2 - r_1^2} \tag{1}$$

$$\sigma_r = -\frac{r_1^2 r_2^2 P_i}{r_2^2 - r_1^2}\frac{1}{r^2} - \frac{r_1^2 P_i}{r_2^2 - r_1^2} \tag{2}$$

$$\sigma_z = P_z - \frac{r_1^2 P_i}{r_2^2 - r_1^2} \tag{3}$$

where σ_θ and σ_r are the hoop stress and radial stress, respectively; σ_z is the axial stress; r_1 and r_2 are the inner radius of rock and the outer radius of rock, respectively; r is the distance of the observed point to the opening center; P_i is the generated equivalent inner pressure; and P_z is the axial stress generated from the loading platen; θ is the angle of the observed line between the horizontal line. It is worth noting that positive value of stress is denoted as compressive stress, while negative one is tensile stress.

It is indicated that the radial stress is compressive, which is zero at $r=r_2$ and equals P_i at $r=r_1$. On the contrary, the hoop stress is in tensile fashion in the specimen, and the values at $r=r_1$ and $r=r_2$ are given by:

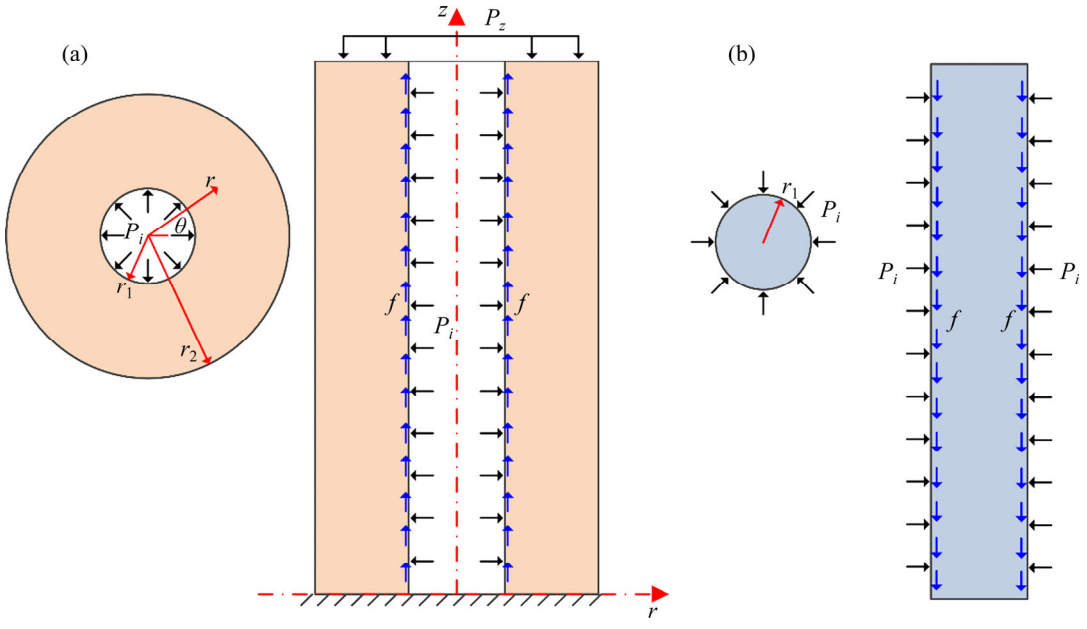

Figure 10 Mechanical model of hollow specimen with filling rod: (a) Hollow cylinder; (b) Filling rod

$$\sigma_\theta\big|_{r=r_2}=-\frac{2r_1^2P_i}{r_2^2-r_1^2} \tag{4}$$

$$\sigma_\theta\big|_{r=r_1}=-\frac{(r_2^2+r_1^2)P_i}{r_2^2-r_1^2} \tag{5}$$

Figure 11 illustrates the distributions of the hoop stress and radial stress along the radial orientation. The tensile stress at the inner wall is the largest and decreases as r increases. The smallest tensile stress is generated at the outer surface of the specimen. Owing to this phenomenon, failure always begins at the inner wall as observed in Figures 7 and 8. With the increase in the axial stress, the interaction between the filling rod and rock becomes more intensive, and hence resulting in higher inner pressure larger displacement. The radial displacements for the filling rod and rock are given by KANJ et al [46].

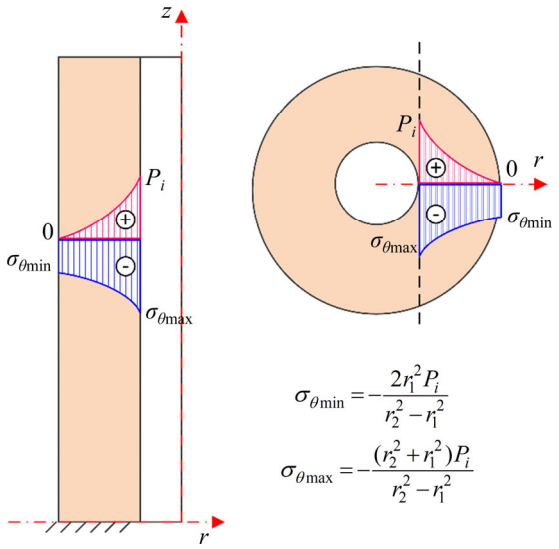

Figure 11 Distributions of hoop stress and radial stress

$$u_{r1}=\frac{(1-\mu_1)P_i}{E_1}r,\ 0<r\le r_1 \tag{6}$$

$$u_{r2}=\frac{(1-\mu_2)r_1^2P_i}{E_2(r_2^2-r_1^2)}r-\frac{(1+\mu_2)r_1^2r_2^2P_i}{E_2(r_2^2-r_1^2)}\frac{1}{r}+\frac{\mu_2P_z}{E_2}r,\ r_1\le r\le r_2 \tag{7}$$

where u_{r1} and u_{r2} are the radial displacements of the filling rod and the rock cylinder, respectively; E_1 and E_2 are the elastic moduli of the filling rod and the rock, respectively; and μ_1 and μ_2 are the Poisson ratio of the filling rod and the rock, respectively. It is worth noting that because the filling rod is stuck to the inner wall, the displacement continuity condition should be satisfied, as is written by:

$$u_{r1}\big|_{r=r_1}=u_{r2}\big|_{r=r_1} \tag{8}$$

Substituting Eqs. (6) and (7), it gives

$$P_i=\frac{\mu_2(k^2-1)P_z}{e(1-\mu_1)(k^2-1)+(1-\mu_2)+(1+\mu_1)k^2} \tag{9}$$

where e is the ratio of E_2 to E_1, $e=E_2/E_1$; and k is the ratio of outer radius to inner radius, $k=r_2/r_1$.

Based on Eq. (9), the inner pressure can be theoretically calculated, which is not only related to the physical mechanical parameters of the filling rod and rock, such as the elastic modulus and Poisson ratio, but also affected by the geometry of the hollow cylinder (i.e., the inner radius and outer radius). When the parameters of the filling material and the rock are known, the inner pressure has a positive linear association with the axial stress. Thus, the normalized inner pressure P_i is expressed as:

$$\bar{P}_i=\frac{P_i}{P_z}=\frac{\mu_2(k^2-1)}{e(1-\mu_1)(k^2-1)+(1-\mu_2)+(1+\mu_1)k^2} \tag{10}$$

To understand the factors that influence the normalized inner pressure, Figure 12 shows the

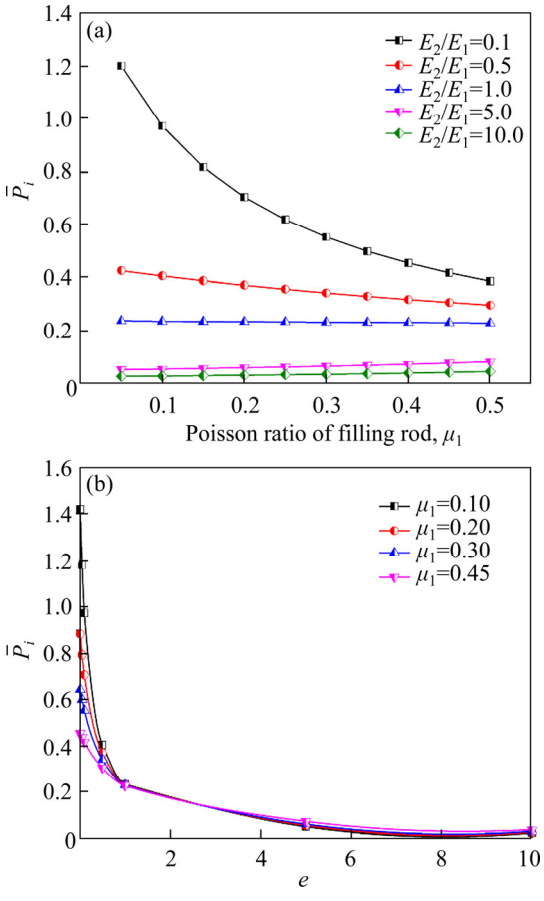

Figure 12 Changes in normalized inner pressure against μ_1 and e: (a) Relationship between $\bar{P}_i$ and μ_1; (b) Relationship between $\bar{P}_i$ and e

changes in normalized inner pressure against varying physical parameters. Based on the parameters of the test specimen, the ratio of outer radius to inner radius is obtained as 3.7, and the Poisson ratio for the test sandstone is 0.25. Figure 12 indicates that for a constant value of μ_1, $\overline{P}_i$ decreases in an exponential manner with the increase of e, and the decreasing rate is large at first and then slows down as e increases. However, for a constant value of e, the change in $\overline{P}_i$ against μ_1 is complicated. Specifically, when e is as low as 0.1, $\overline{P}_i$ decreases exponentially with the increase in μ_1. When e becomes larger, for instance 0.5 or higher, $\overline{P}_i$ decreases in an approximately linear manner with increasing μ_1. The results indicate that the change in $\overline{P}_i$ is more sensitive to the parameter e than μ_1. Therefore, a higher $\overline{P}_i$ will be induced in the filling rod with a higher elastic modulus and higher Poisson ratio.

In terms of the filling materials used in this study, the values of $\overline{P}_i$ can be obtained based on the parameters given in Table 1 and Eq. (10). Figure 13 presents the values of $\overline{P}_i$ and the relationship of P_i with P_z for the three filling materials. It indicates that more intensive inner pressure is generated in the inner wall of the hollow cylinder filled with Al. This can be the reason that the UCS of HC-Al is much lower than that of HC-Pb and HC-PMMA as shown in Figure 4. An interesting phenomenon a observed in Figure 4 is that the UCS of HC-PMMA is subtly greater than that of the solid specimen. As indicated in Figure 13, the inner pressure for HC-PMMA is merely 0.0616 times the axial stress. This finding indicates that a small inner pressure in the hollow specimen helps to promote the overall strength, while a larger inner pressure results in lower strength

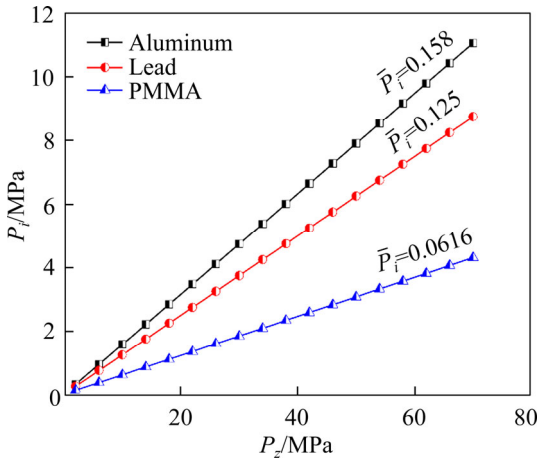

Figure 13 Relationships of P_i with P_z for three filling materials

of the specimen (for instance HC-Al and HC-Pb). This can be further justified from the results obtained by WANG et al [26], in which it is found that a moderate internal pressure clearly improves the bearing capacity of the hollow cylinder, while a high internal pressure induces local failure at the inner wall and hence weakening the bearing capacity of the rock specimen.

5 Conclusions

In this study, unconfined compression tests were conducted on hollow specimens with filling materials (i.e., HC-AL, HC-Pb, HC-PMMA), as well as hollow cylindrical (HC) and solid cylindrical (SC) specimens. The influences of the infillings on the UCS, elastic modulus and failure pattern of the hollow specimens with infillings was investigated. The interactions of the filling rod and rock were studied by strain gauge measurements and theoretical analyses. The results indicated that the UCS and elastic modulus for the solid and hollow specimens are similar, and the centre hole exerts insignificant effects of changing the mechanical behaviors of solid and hollow specimens. However, both the UCS and elastic modulus of the filled hollow specimen decrease with increasing the stiffness of the filling material. The interaction of the filling rod with the rock structure initiates at the early stage of elastic deformation (30% UCS) and the localized failure occurs at the end of the elastic deformation (70% UCS). In addition, a higher hoop stress will be induced in the filling material with a higher stiffness, hence leading to a higher interfacial stress. Finally, the theoretical analyses suggest that a higher equivalent inner pressure will be induced in the inner wall with a higher elastic modulus and higher Poisson ratio of the filling material. A small inner pressure in the hollow cylinder helps to promote the overall strength of the specimen, while a larger inner pressure results in lower strength of the specimen.

Contributors

WU Qiu-hong provided the concept and edited the draft of manuscript. WENG Lei conducted the literature review and wrote the first draft of the manuscript. ZHAO Yan-lin and FENG Fan edited the draft of manuscript.

Conflict of interest

WU Qiu-hong, WENG Lei, ZHAO Yan-lin and FENG Fan declare that they have no conflict of interest.

References

[1] KAHRAMAN S. Evaluation of simple methods for assessing the uniaxial compressive strength of rock [J]. International Journal of Rock Mechanics and Mining Sciences, 2001, 38(7): 981−994. DOI: 10.1016/S1365-1609(01)00039-9.

[2] MOGI K. Fracture and flow of rocks under high triaxial compression [J]. Geophysical research, 1971, 76(5): 1255−1269. DOI: 10.1029/JB076i005p01255.

[3] ZHOU Xiao-ping, CHENG Hao, FENG Yi-feng. An experimental study of crack coalescence behaviour in rock-like materials containing multiple flaws under uniaxial compression [J]. Rock Mechanics and Rock Engineering, 2014, 47(6): 1961−1986. DOI: 10.1007/s00603-013-0511-7.

[4] ZHOU Xiao-ping, ZHANG Jian-zhi, WONG L N Y. Experimental study on the growth, coalescence and wrapping behaviors of 3d cross-embedded flaws under uniaxial compression [J]. Rock Mechanics and Rock Engineering, 2018, 51(5): 1379−1400. DOI: 10.1007/s00603-018-1406-4.

[5] PENG Kang, LIU Zhao-peng, ZOU Quan-le, WU Qiu-hong, ZHOU Jia-qi. Mechanical property of granite from different buried depths under uniaxial compression and dynamic impact: An energy-based investigation [J]. Powder Technology, 2020, 362: 729−744. DOI: 10.1016/j.powtec. 2019.11.101.

[6] ZHAO Yan-lin, WANG Yi-xian, WANG Wei-jun, WAN Wen, TANG Jing-zhou. Modeling of non-linear rheological behavior of hard rock using triaxial rheological experiment [J]. International Journal of Rock Mechanics and Mining Sciences, 2017, 93: 66−75. DOI: 10.1016/j.ijrmms.2017.01.004.

[7] WU Qiu-hong, WENG Lei, ZHAO Yan-lin, GUO Bao-hua, LUO Tao. On the tensile mechanical characteristics of fine-grained granite after heating/cooling treatments with different cooling rates [J]. Engineering Geology, 2019, 253: 94−110. DOI: 10.1016/j.enggeo.2019.03.014.

[8] WU Qiu-hong, CHEN Lu, SHEN Bao-tang, DLAMINI B, LI Shu-qing, ZHU Yong-jian. Experimental investigation on rockbolt performance under the tension load [J]. Rock Mechanics and Rock Engineering, 2019, 52(11): 4605−4618. DOI: 10.1007/s00603-019-01845-1.

[9] DU Kun, SU Rui, TAO Ming, YANG Cheng-zhi, MOMENI A, WANG Shao-feng. Specimen shape and cross-section effects on the mechanical properties of rocks under uniaxial compressive stress [J]. Bulletin of Engineering Geology and the Environment, 2019, 78: 6061−6074. DOI: 10.1007/ s10064-019-01518-x.

[10] HUDSON J A, CROUCH S L, FAIRHURST C. Soft, stiff and servo-controlled testing machines: A review with reference to rock failure [J]. Engineering Geology, 1972, 6(3): 155−189. DOI: 10.1016/0013-7952(72)90001-4.

[11] ZHANG Zi-zheng, DENG Ming, BAI Jian-biao, YAN Shuai, YU Xian-yang. Stability control of gob-side entry retained under the gob with close distance coal seams [J]. International Journal of Mining Science and Technology, 2021. DOI: 10.1016/j.ijmst.2020.11.002.

[12] XUE Lei, QIN Si-qing, SUN Qiang, WANG Yuan-yuan, LEE Min, LI Wei-chao. A study on crack damage stress thresholds of different rock types based on uniaxial compression tests [J]. Rock Mechanics and Rock Engineering, 2014, 47(4): 1183−1195. DOI: 10.1007/s00603-013-0479-3.

[13] ALSAYED M I. Utilising the hoek triaxial cell for multiaxial testing of hollow rock cylinders [J]. International Journal of Rock Mechanics and Mining Sciences, 2002, 39: 355−366. DOI: 10.1016/S1365-1609(02)00030-8.

[14] SANTARELLI F J, BROWN E T. Failure of Three sedimentary rocks in triaxial and hollow cylinder compression tests [J]. International Journal of Rock Mechanics and Mining Sciences and Geomechanics Abstracts, 1989, 26(5): 401−413. DOI: 10.1016/0148-9062(89)90936-4.

[15] WENG Lei, HUANG Lin-qi, TAHERI A, LI Xi-bing. Rockburst characteristics and numerical simulation based on a strain energy density index: A case study of a roadway in linglong gold mine, China [J]. Tunnelling and Underground Space Technology, 2017, 69: 223−232. DOI: 10.1016/j.tust.2017.05. 011.

[16] DIEDERICHS M S, KAISER P K, EBERHARDT E. Damage initiation and propagation in hard rock during tunnelling and the influence of near-face stress rotation [J]. International Journal of Rock Mechanics and Mining Sciences, 2004, 41: 785−812. DOI: 10.1016/j.ijrmms.2004.02.003.

[17] ZHANG Zi-zheng, DENG Ming, WANG Xiang-yu, YU Wei-jian, ZHANG Fei, DAO V D. Field and numerical investigations on the lower coal seam entry failure analysis under the remnant pillar [J]. Engineering Failure Analysis, 2020, 115: 104638. DOI: 10.1016/j.engfailanal.2020.104638.

[18] WU Qiu-hong, LI Xi-bing, WENG Lei, LI Qing-feng, ZHU Yong-jian, LUO Rong. Experimental investigation of the dynamic response of prestressed rockbolt by using an SHPB-based rockbolt test system [J]. Tunnelling and Underground Space Techology, 2019, 93: 103088. DOI: 10.1016/j.tust. 2019.103088.

[19] TAO Ming, MA Ao, CAO Wen-zhuo, LI Xi-bing, GONG Feng-qiang. Dynamic response of pre-stressed rock with a circular cavity subject to transient loading [J]. International Journal of Rock Mechanics and Mining Sciences, 2017, 99: 1−8. DOI: 10.1016/j.ijrmms.2017.09.003.

[20] ZHOU Xiao-ping, ZHANG Yong-xing, HA Qiu-ling. Real-time computerized tomography (CT) experiments on limestone damage evolution during unloading [J]. Theoretical and Applied Fracture Mechanics, 2008, 50(1): 49−56. DOI: 10.1016/j.tafmec.2008.04.005.

[21] ZHOU Xiao-ping, SHOU Yun-dong, QIAN Qi-hu. Three-dimensional nonlinear strength criterion for rock-like materials based on the micromechanical method [J]. International Journal of Rock Mechanics and Mining Sciences, 2014, 72: 54−60. DOI: 10.1016/j.ijrmms.2014.08.013.

[22] LI Jun-zhe, ZHANG Guang, LIU Ming-ze. Experimental investigation on the effect of confining pressure on the tensile strength of sandstone using hollow cylinder tensile test method [J]. Arabian Journal of Geosciences, 2019, 12: 768.

DOI: 10.1007/s12517-019-4797-y.

[23] LABIOUSE V, SAUTHIER C, YOU S. Hollow cylinder simulation experiments of galleries in boom clay formation [J]. Rock Mechanics and Rock Engineering, 2014, 47(1): 43−55. DOI: 10.1007/s00603-012-0332-0.

[24] YANG Sheng-qi. Experimental study on deformation, peak strength and crack damage behavior of hollow sandstone under conventional triaxial compression [J]. Engineering Geology, 2016, 213: 11−24. DOI: 10.1016/j.enggeo.2016.08.012.

[25] WU Qiu-hong, LI Xi-bing, ZHAO Fu-jun, TAO Ming, DONG Long-jun, CHEN Lu. Failure characteristics of hollow cylindrical specimens of limestone under hole pressure unloading [J]. Chinese Journal of Rock Mechanics and Engineering, 2017, 36(6): 1424−1433. DOI: 10.13722/j.cnki.jrme.2016.1498. (in Chinese)

[26] WANG Shao-feng, LI Xi-bing, DU Kun, WANG Shan-yong, TAO Ming. Experimental study of the triaxial strength properties of hollow cylindrical granite specimens under coupled external and internal confining stresses [J]. Rock Mechanics and Rock Engineering, 2018, 51(3): 1−17. DOI: 10.1007/s00603-018-1452-y.

[27] ZHOU Hui, JIANG Yue, LU Jing-jing, GAO Yang, CHEN Jun. Development of a hollow cylinder torsional apparatus for rock [J]. Rock Mechanics and Rock Engineering, 2018, 51(12): 3845−3852. DOI: 10.1007/s00603-018-1563-5.

[28] ADAMS F D. An experimental contribution to the question of the depth of the zone of flow in the earth's crust [J]. Journal of Geology, 1912, 20(2): 97−118.

[29] KING L V. On the Limiting strength of rocks under conditions of stress existing in the earth's interior [J]. Journal of Geology, 1912, 20(2): 119−138.

[30] TALESNICK M L, RINGEL M. Completing the hollow cylinder methodology for testing of transversely isotropic rocks: torsion testing [J]. International Journal of Rock Mechanics and Mining Sciences, 1999, 36(5): 627−639. DOI: 10.1016/S0148-9062(99)00038-8.

[31] HAIMSON B, KOVACICH J. Borehole instability in high-porosity berea sandstone and factors affecting dimensions and shape of fracture-like breakouts [J]. Engineering Geology, 2003, 69: 219−231. DOI: 10.1016/S0013-7952(02)00283-1.

[32] MONFARED M, DELAGE P, MOHAJERANI M. A laboratory investigation on thermal properties of the opalinus claystone [J]. Rock Mechanics and Rock Engineering, 2011, 44(6): 735−747. DOI: 10.1007/s00603-011-0171-4.

[33] GAY N C. Fracture growth around openings in thick-walled cylinders of rock subjected to hydrostatic compression [J]. International Journal of Rock Mechanics and Mining Sciences and Geomechanics Abstracts, 1973, 10: 231–243. DOI: 10.1016/0148-9062(73)90032-6.

[34] YOU Ming-qing, SU Cheng-dong, GOU Yong. Experimental study on strength and deformation properties of hollow cylindrical specimens of marbles [J]. Chinese Journal of Rock Mechanics and Engineering, 2007, 26(12): 2420−2429. DOI: 10.1016/S1874-8651(08)60066-6. (in Chinese)

[35] ZHANG Hou-quan, LIU Hong-gang, HE Yong-nian, HAN Li-jun. Unloading experiment and rock strength failure of rock thick-walled cylinders under triaxial compression [J] .Journal of University of Science and Technology Beijing, 2011, 33(7): 800−805. DOI: 10.1097/RLU.0b013e3181f49ac7.

[36] LABIOUSE V, VIETOR T. Laboratory and in situ simulation tests of the excavation damaged zone around galleries in opalinus clay [J].Rock Mechanics and Rock Engineering, 2014, 47(1): 57−70. DOI: 10.1007/s00603-013-0389-4.

[37] LI Zhen, ZHOU Hui, JIANG Yue, HU Da-wei, ZHANG Chuan-qing. Methodology for establishing comprehensive stress paths in rocks during hollow cylinder testing [J]. Rock Mechanics and Rock Engineering, 2019, 52: 1055−1074. DOI: 10.1007/s00603-018-1628-5.

[38] QIU Jia-dong, LI Di-yuan, LI Xi-bing, ZHU Quan-qi. Numerical investigation on the stress evolution and failure behavior for deep roadway under blasting disturbance [J]. Soil Dynamics and Earthquake Engineering, 2020, 137: 106278. DOI: 10.1016/j.soildyn.2020.106278.

[39] SU Cheng-dong, QIU Jia-dong, WU Qiu-hong, WENG Lei. Effects of high temperature on the microstructure and mechanical behavior of hard coal [J]. International Journal of Mining Science and Technology, 2020, 30(5): 643−650. DOI: 10.1016/j.ijmst.2020.05.021.

[40] WENG Lei, WU Qiu-hong, ZHAO Yan-lin, WANG Shi-ming. Dynamic response and failure of rock in initial gradient stress field under stress wave loading [J]. Journal of Central South University, 2020, 27: 963−972. DOI: 10.1007/s11771-020-4344-8.

[41] WU Qiu-hong, LI Xi-bing, TAO Ming, ZHAO Fu-jun, WENG Lei, DONG Long-jun. Conventional triaxial compression on hollow cylinders of sandstone with various fillings: Relationship of surrounding rock with support [J]. Journal of Central South University, 2018, 25(8): 1976−1986. DOI: 10.1007/s11771-018-3888-3.

[42] GOU Yong, PEI Hong-yan, WU Zhen-hua. Study on strength, deformation and failure properties of hollow cylindrical rock specimens [C]// International Conference on Energy and Environmental Protection, 2017.

[43] CAI M, KAISER P K, TASAKA Y, MAEJIMA T, MORIOKA H, MINAMI M. Generalized crack initiation and crack damage stress thresholds of brittle rock masses near underground excavations [J]. International Journal of Rock Mechanics and Mining Sciences, 2004, 41(5): 833−847. DOI: 10.1016/j.ijrmms.2004.02.001.

[44] WU Qiu-hong, WENG Lei, ZHAO Yan-lin, ZHAO Fu-jun, ZHANG Si-ping. Deformation and cracking characteristics of ring-shaped granite with inclusion under diametrical compression [J]. Arabian Journal of Geosciences, 2020, 13: 681. DOI: 10.1007/s12517-020-05718-8.

[45] HASHEMI S S, MELKOUMIAN N, TAHERI A. A borehole stability study by newly designed laboratory testson thick-walled hollow cylinders [J]. Journal of Rock Mechanics Geotechnical Engineering, 2015, 7(5): 519−531. DOI: 10.1016/j.jrmge.2015.06.005

[46] KANJ M, ABOUSLEIMAN Y. The generalized lame problem—part I: Coupled poromechanical solutions [J]. Journal of Application Mechanics, 2004, 71: 168−179. DOI: 10.1115/1.1683751.

(Edited by ZHENG Yu-tong)

中文导读

单轴压缩下不同刚度充填物对厚壁圆筒砂岩力学及断裂响应的影响

摘要：为了研究不同刚度充填物对厚壁圆筒砂岩力学及断裂响应的影响，对充填铝棒、铅棒以及有机玻璃棒的厚壁圆筒砂岩试样进行单轴压缩试验，同时对完整砂岩试样及厚壁圆筒试样也进行单轴压缩试验作为参照。对比研究各组试样的强度、变形及破坏特征，并通过岩石和充填棒上的环向应变值特征分析了影响应力阈值及局部破坏应力阈值的变化情况。研究结果表明，完整试样和厚壁圆筒试样的强度及弹性模量没有明显的差别，而充填试样的强度随着充填物刚度的增加而减小。刚度较大的充填物导致试样产生较大的环向应力，进而产生较大的界面力。充填试样以拉伸破坏为主，而完整试样及厚壁圆筒试样主要为剪切破坏。最后通过理论力学模型研究孔洞内壁的等效内压力，发现理论模型能够很好地解释试验结果。本文研究结果将为非均匀应力状态下岩体及支护结构的稳定性提供有意义参考。

关键词：力学特征；厚壁圆筒；充填物；环形应力；单轴压缩